Nano Select

WILEY-VCH

RESEARCH ARTICLE OPEN ACCESS

Production of Biodiesel from Crude *Pittosporum resiniferum* Oil Using Heterogeneous Solid Base Catalyst

Rogers Kipkoech | Mohammed Takase

Department of Environmental Science, School of Biological Sciences, University of Cape Coast, Cape Coast, Ghana

Correspondence: Rogers Kipkoech (rogers.kipkoech@stu.ucc.edu.gh)

Received: 4 September 2023 | **Revised:** 21 May 2024 | **Accepted:** 3 June 2024

Funding: The authors received no specific funding for this work.

Keywords: biodiesel | characterize | heterogeneous catalyst | *Pittosporum resiniferum* | transesterification

ABSTRACT

Pittosporum resiniferum oil was extracted from the seed and the oil together with methanol was use for the production of biodiesel through transesterification process using novel solid base catalyst (K_2CO_3 supported on MgO). 0.6:5 (K_2CO_3 loaded on MgO), a 5 h calcination time, 600°C calcination temperatures were the optimum conditions under which the catalyst was prepared. FTIR, SEM, CO_2-TPD, XRD, N2 adsorption-desorption, Hammett indicators and other techniques were used to characterize the catalyst. The molar ratio of methanol-to-oil, the catalyst amount, time of the reaction as well as the temperature of the reaction were examined. The study found that 16:1 methanol-to-oil molar ratio, 5% catalyst loading amount, a reaction time of 2.0 h, and a reaction temperature of 60°C were sufficient for a maximum yield of 97.4%. With relative high activity, the catalyst can perhaps be used again possibly for five times. The characteristics of the biodiesel produced were consistent with international standards.

1 | Introduction

The ongoing increase in the worldwide prices of fuel obtained from fossil sources, in addition to the declining storage of traditional energy supplies and its accompanying environmental related issues, has raised awareness of various sustainable and renewable fuel alternatives for the fuel sector [1, 2]. Biodiesel is produced mostly from vegetable oil sources such as mono-alkyl esters, and is one of the most viable alternatives to conventional diesel.

Biodiesel is quickly becoming a preferred biofuel globally [3, 4]. Biodiesel has several benefits over conventional fuel, which include being renewable, low emissions, biodegradable, great lubricity and a high flash point [5]. Biodiesel also lowers pollution levels [6] and can be blended with diesel or utilized in its original form [7, 8].

Alkaline, acid, and enzymes are usually used as catalysts to trans esterify vegetable oils [9, 10]. Alkaline catalysts are classified as either homogeneous or heterogeneous. Biodiesel is produced on a commercial scale using a homogenous base (NaOH or KOH). The advantages of heterogenous catalysts include; its catalytic activity that makes it reuseable after reaction, faster rate of reactions and selectivity's, easy separation of products and catalysts and the low cost. As a result of these factors catalysts for transesterification are increasingly receiving attention globally [9, 11, 12]. Unfortunately, use of homogenous base catalyst has disadvantages which include corrosion of the equipment and trash generation through acid neutralization. The acid catalyst alternatively, uses a lot of energy and takes a long time to react. Alternatively heterogenous catalysts in nature are environmentally friendly [11]. Kulkarni et al. [13] and Laosiripojana et al. [14] evaluated heteropoly acid impregnated on various supports (zirconia, silica, activated carbon and alumina), SO_4-ZrO_2 and WO_3-ZrO_2 for biodiesel

This is an open access article under the terms of the Creative Commons Attribution License, which permits use, distribution and reproduction in any medium, provided the original work is properly cited.

© 2024 The Author(s). *Nano Select* published by Wiley-VCH GmbH.

obtained from canola oil by employing acid catalyst in solid form. Heterogeneous solid acid has challenges that arises due to higher temperatures required and longer reaction time.

Using incipient impregnation method to load SrO [14], CaO [13], and KNO_3 on flash [14], ZnO—La_2O_3 [15] and zinc aluminate [16] respectively, have demonstrated that heterogeneous solid base catalysts for the production of the biodiesel are promising. Most of the heterogeneous solid base catalysts have been used in the transesterification of edible oils [17] which compounds the present rise in global food consumption [18]. Some alternative heterogeneous catalysts are too costly due to process of their preparation.

Pittosporum resiniferum, often referred as "petroleum nut" or "abakel" in Tagalog, was used in this work. *P. resiniferum* is a member of the Pittosporaceae family of plants. The plant is indigenous species which is native to Philippines and has spread to south and west Africa, particularly South Africa and Ghana. Its blossoms as aromatic and delicious plant. *P. resiniferum* is a parasitic fungus that develops on trees. It is often cultivated at altitudes ranging from 900 to 2400 meters in mossy woods. *P. resiniferum* is distinguished by a high concentration of resin compounds its fruit. *P. resiniferum* has fruit with the length of about 30 mm and thickness of 23 mm. The seed oil obtained from fruit is intriguing since it contained a considerable level of typical heptane. According to available studies, the plant generates a lot of oil. However, little is known on the possibility of using the oil for producing green energy (biodiesel) [19]. The study therefore, seeks to investigate production of biodiesel from *P. resiniferum* oil that can be sustainable and less competitive substitute to conventional diesel fuel using heterogeneous solid base catalyst which is easily separated from the reaction mixture, therefore, reducing the need for additional purification steps and hence reducing negative environmental impact.

2 | Materials and Methods

2.1 | Materials

Ryte Aid Pharmaceutical Co., Ltd, situated in Ho, Ghana, supplied the *P. resiniferum* seeds (Plate 1) as well as methanol, MgO, K_2CO_3, Al_2O_3, TiO_2, CaO, SnO_2, ZrO_2, and SiO_2. All the solvents used were graded by AR and there was no need to purify further.

2.2 | Oil Extraction

Drying of *P. resiniferum* seeds was carried in an oven at temperature of 110°C for 8 h before to extraction to eliminate excess moisture. The dried seeds were then weighed and crushed into 0.5–10 mm particles. Petroleum ether (60–90°C) was used to extract the oil from the seeds, using a soxhlet extractor (Plate 2). Each extraction batch took 9 h to complete. A kilogram of seed was subjected to the extraction using 5 L of the solvent. The oil was extracted and was then recovered by means of a rotary evaporator. The quantity of oil in the seeds was assessed following the procedure provided by Takase et al. [20]. The subsequent determination and identification of fatty acids composition was carried out using GC-MS (Plate 3).

2.3 | Catalysts Preparation

The solid-state approach was used to provide a simple way for producing catalysts (K_2CO_3) supported on carriers. All the carriers were off-the-shelf items that were utilized without treatment. K_2CO_3 and carriers were therefore, combined using a ratio of K_2CO_3/MgO is x/1 (x = 0, 0.1,0.2, 0.4, 0.6, and 0.8) in a mortar and skived for 30 min. The mixture was then dried using hot air in oven at a temperature of 80°C for a period of 4 h. Catalyst was produced after calcination at temperature of 600°C for 4 h in a heat ratio of 1°C min^{-1} in air.

2.4 | Catalysts' Characterization

Using a Fourier Transform Infrared Spectroscopy (FTIR) (AVATAR 360, Nicolet, Madison, USA), the samples' FTIR spectra were acquired on KBr powder between 4000 and 500 cm^{-1}, 32 scans in total were carried out, 2 cm^{-1} resolution was in the range of 4000–500 cm^1.

Images were taken utilizing a 20-kV accelerating voltage field emission scanning electron microscope (S-4800, HITACHI Corp., Tokyo, Japan). The nitrogen absorbance technique with the NDVA2000e analytical instrument (Quntachrome Corporation USA) was used to characterize the Brunauer–Emmett–Teller (BET) values of the surface area of the particles of the catalyst particles and was followed by computing of the specific surface area. Barrett-Joyner-Halenda (BJH) technique, was used to estimate the size, distribution, and volume of the pore. The samples were left over the night in an oven at 120°C under vacuum before being measured for surface area [22].

Gravimetric determination of carbon dioxide uptake at 300, 350, 375, and 400°C at atmospheric pressure was carried out through use of a thermogravimetric analyser (Mettler Toledo TGA-SDTA851). Calcined adsorbents were initially activated at 450°C with a temperature ramp rate of 10°C min^{-1} and kept at 450°C for 60 min under nitrogen flow before temperature reduction to the corresponding adsorption temperatures at a rate of −5°C min^{-1} and kept at the adsorption temperature for another 15 min with nitrogen flow. The gas was thereafter switched to CO_2 for the adsorption phase. The time of adsorption that was set was 120 min in which a near equilibrium adsorption state could be obtained [23–26].

Experiments using Hammett indicators were carried out to establish the strength of alkalinity of each catalyst [23, 24]. Phenolphthalein (H = 9.8), Bromothymol blue (H = 7.2), 4-nitroaniline (H = 18.4) and 2,4-dinitroaniline (H = 15) were utilized as markers. Catalyst weighing 300 mg was combined with a solution of 1 mL of Hammett indicator which had undergone dilution in 10 mL methanol and was then left to settle for 2.5 h. Catalyst's color was observed at the end of the reaction. The color change represents the neutralization point, which is where the basic sites on the catalyst react with the acid. Specifically, the color appearing is determined by the value of indicator's pKa, that correlates to the strength of the catalyst's basic sites. The color of the indicator suggests the existence and amount of basic sites on the K_2CO_3/MgO catalyst, and this gives vital information on its



PLATE 1 | *Pittosporum resiniferum* (petroleum nut) (A- fresh sample, B- nuts with seed, C- nuts without seeds and D- dried nuts) [21].



PLATE 2 | Extraction of *Pittosporum resiniferum* oil using a soxhlet extractor. *Source*: Authors, 2023.



PLATE 3 | GC-MS machine. *Source*: Authors, 2023.

catalytic characteristics and efficiency in reactions. According to the results, the basic strength of the catalyst was higher as compared to the weakest indicator that changed the color and lower as compared to the strongest indicator which did not change the color. The determination of the basicity of the solid catalyst was carried through the use of Hammett indicator benzene carboxylic acid (0.02 mol L^{-1} anhydrous ethanol solution) titration procedure [24–26].

2.5 | Transesterification of *Pittosporum resiniferum* Oil to Biodiesel

The triglycerides were trans esterified to fatty acid methyl esters (FAMEs) through the use of 30 g of extracted oil, varying molar ratio of methanol to oil (9:1–17:1), and various concentrations of the catalyst (3%, 5%, 7%, 9%, 11%) relative to the oil's weight at

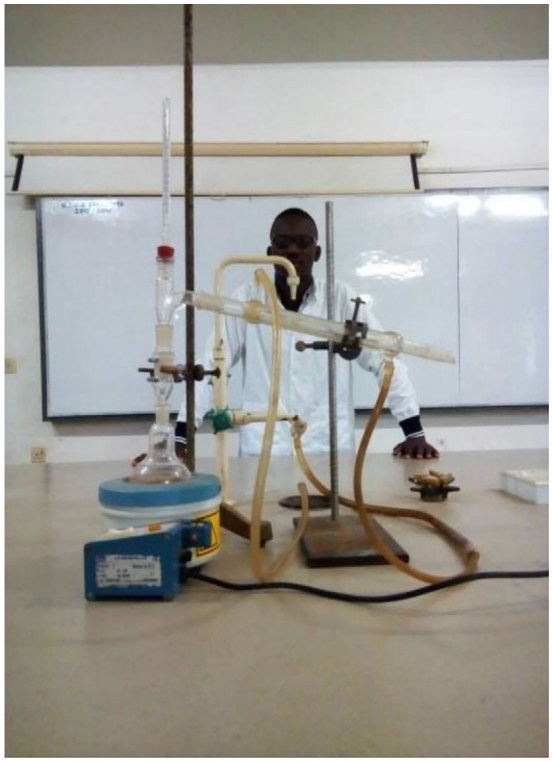


PLATE 4 | Biodiesel production setup. *Source*: Authors, 2023.

varying temperatures (40, 50, 60, 65, and 70°C), and time (1–3 h), and refluxing were carried out on these together in a 250 mL three-neck flask for the reaction fitted with a condenser and magnetic stirrer (600 rpm) (Plate 4). Hexane was used to rinsed the mixture after each reaction to eliminate any incorporated FAMEs from the solid catalyst. The mixture was then centrifuged, thereafter, for 10 min at 5000 rpm to separate the catalyst in solid form from the layer of the liquid that included the biodiesel and n-hexane. Decanting and transportation of the biodiesel to a rotary vacuum evaporator was done in order to remove the n-hexane and any other by-products. Each biodiesel sample was then placed in a separating funnel and left for 24 h before being washed three times with water. Biodiesel was then dried and analyzed (Plate 5).

2.6 | Analyses of Biodiesel Yields

A 7890A gas chromatograph (Agilent Technology Inc., USA) with a flame-ionization detector (FID) and an HP-5 capillary column (30 m × 0.32 mm 0.25 μm) was used to analyze the biodiesel samples. Carrier gas, helium was utilized. The temperature of the oven ramp program was run by initially keeping the temperature at 160°C for 1 min, then increasing to a temperature of 210°C at 20°C min^{-1} for 2 min, again increasing it from 210°C to 213°C at 0.3°C min^{-1} within 3 min, and lastly increasing it to 250°C at 30°C min^{-1} for a period of 1 min. The hydrogen gas and air flow rate were 40 mL min^{-1} and 400 mL min^{-1} respectively. The temperature of injector and detector were both at 250°C. The injection was split at a ratio of 100:1. The analysis of every sample was carried out by dissolving 1 mL of biodiesel in 5 mL of petroleum ether (30–60°C) in the presence of tetradecane as



PLATE 5 | Biodiesel samples obtained from *Pittosporum resiniferum* oil.

an internal standard, then injecting 0.5 L of the solution into GC. Using the equation below, the yield of each biodiesel sample was calculated based on the concentration of esters:

$$Biodiesel\ yield = \frac{W_{tetradecane} \times A_B \times f_{tetradecane}}{A_{tetradecane} \times W_s} \times 100\% \quad (1)$$

where $W_{tetradecanee}$ is the weight of tetradecane, $f_{tetradecane}$ is the response factor, A_B is the peak area of methyl esters, $A_{tetradecane}$ is the peak area of tetradecane, and W_s is the weight of the sample.

The reported data are the mean (values) of three replicate experiments and GC assessments.

Properties of biodiesel were analyzed using the ASTM 6751 Standard and European Standard (14214). Properties that were analyzed included; cetane number (ASTM D6890-07), kinematic viscosity (ASTM D445-06), Oxidative stability 110°C (h) (EN 14112), pour point (GB/T3535), flash point (ASTM D93-07), sulphur content (ASTM D4294), ash content (GB/T508), acid value (ASTM D664-01), water/moisture content (ASTM D6304), density at (20°C) (SH/T0248), and total glycerine (SH/T0796), were determined.

2.7 | Identification of the Fatty Acid Methyl Esters

An Agilent HP-6890 gas chromatograph (Agilent Technologies, Palo Alto, CA, USA) equipped with an HP-5MS 5% phenylmethylsiloxane capillary column (30 m 0.25 mm i.d., film thickness 0.25 m; Restek, Bellefonte, PA) was used to detect the FAMEs. Helium at a flow rate of 1.0 mL min^{-1} was used as the carrier gas. Every sample of the biodiesel (1 μL) was fed into the column at a split ratio of 100:1. The GC (*Procedure 2.6*) approach was used

TABLE 1 | The composition of fatty acid of the *Pittosporum resiniferum* seed oil.

Acidity index	Palmitic (C16:0)	Stearic (C18:0)	Oleic (C18:1)	Linoleic (C18:3)	Linoleic (C18:2)
Composition (wt%)	10	3	25	10	52

TABLE 2 | Physicochemical properties of *Pittosporum resiniferum* seed oil.

Property	Testing procedure	ASTM Std.	Determined value
Density at 20°C (kg/m^3)	ASTMD4052-96	860–890	916.2
Saponification value (mgKOH/g)	ASTMD4052-96	191–202	191.65
Kinematic viscosity at 40°C (mm^2/s)	ASTMD 445-06	1.9–6.0	35.70
Water content (%, w/w)	AOAC 984.20-90	0.05 max	0.64
Free fatty acid content (%, w/w)	AOAC 940.28	—	0.082

to execute the oven temperature ramp program. Using AMDIS-Chromatogram (GC-MS system) software, the fatty acids methyl esters were identified through the comparison of the acquired mass spectra with NIST05.LIB and NIST05s.LIB (National Institute of Standards and Technology) libraries data.

3 | Results and Discussion

3.1 | Extraction of Oil

The quantity of oil extracted from the seeds was estimated to be 41%. The value, however, was equivalent to Da Costa Evangelista et al. [27] data, which shows a possibility of being a viable feedstock source for producing biodiesel synthesis [19]. *P. resiniferum* oil was analyzed for fatty acid composition (Table 1) and physicochemical properties which include density, kinematic viscosity, moisture content, and free fatty acid (Table 2).

The free fatty acid and the moisture content of the oil were 0.64 and 0.082 while oil density, saponification value, and kinematic viscosity were, 916.2, 191.65, and 35.70 respectively (Table 2). The significant quantity of free fatty acid and water content that were present in the oils might result in huge quantities of soap, which can reduce ester yields [20]. MgO catalyst was loaded oxide that was selected for this study because K_2CO_3 produced 0% methyl esters from the oil, with free fatty acid and moisture content of 0.64% w/w and 0.085% w/w, respectively (numbers below 1.0%) [28]. The oil's FFA and the moisture content were comparable to earlier studies [23]. The FFA composition of the oil additionally was an important consideration for biodiesel application in diesel engines [29].

Saturated fatty acid esters have a greater cetane number and oxidation stability than unsaturated fatty acid esters, but they have poor cold flow characteristics [30]. The unrefined *P. resiniferum* seed oil has a greater concentration of unsaturated fatty acids, particularly linoleic acid (62%), and a lower proportion of saturated fatty acid (Table 1).

3.2 | Catalyst Characterization

3.2.1 | FTIR and SEM Analysis of K_2CO_3/MgO

FTIR analysis (Figure 1) was performed to explore the active sites of K_2CO_3/MgO, and the findings revealed a breakdown of K_2CO_3 onto MgO. The connection between K_2CO_3 and MgO was visible in the decomposition temperature of K_2CO_3 in K_2CO_3/MgO at 600°C. The decomposition temperature of K_2CO_3 when combined with magnesium oxide (MgO) at 600°C is around 891°C under standard atmospheric conditions. However, MgO presence can affect this process, potentially lowering the temperature due to intermediate compounds [16].

Catalytic activity of K_2CO_3/MgO was substantially greater compared to that of K_2CO_3, even on lowering catalyst quantity, the stronger alkaline site, for example K_2O, could have had a significant influence on the reaction. The K_2CO_3/MgO catalyst band stretching from 3800 to 2200 cm^{-1} regions are endothermic peak possibly as a result of very weak bonding vibration of water molecules.

SEM image of K_2CO_3/MgO catalyst and of MgO alone (the carrier) catalyst is shown in Figure 2. The SEM pictures of K_2CO_3/MgO samples show crystallites with sizes ranging from 0.5 to 1 μm. K_2CO_3 was well dispersed on the surface of MgO. After K_2CO_3 was loaded onto MgO, the catalyst's structure was preserved, and potassium species were detected scattered on the support's surface. The catalyst particle sizes ranged from 10 to 100 μm, according to the K_2CO_3/MgO picture.

The higher particle sizes of the catalyst provided more active sites, hence promoting greater chance of collisions between the reactants and the catalyst, thus increasing the rate of transesterification reaction [31, 32].

The load relationship of K_2CO_3/MgO as shown by Scanning Electron Microscopy (SEM) in Figure 2A indicates how K_2CO is distributed and interacts on the surface of MgO. The SEM image (Figure 2A) gives the typical highlights of the following

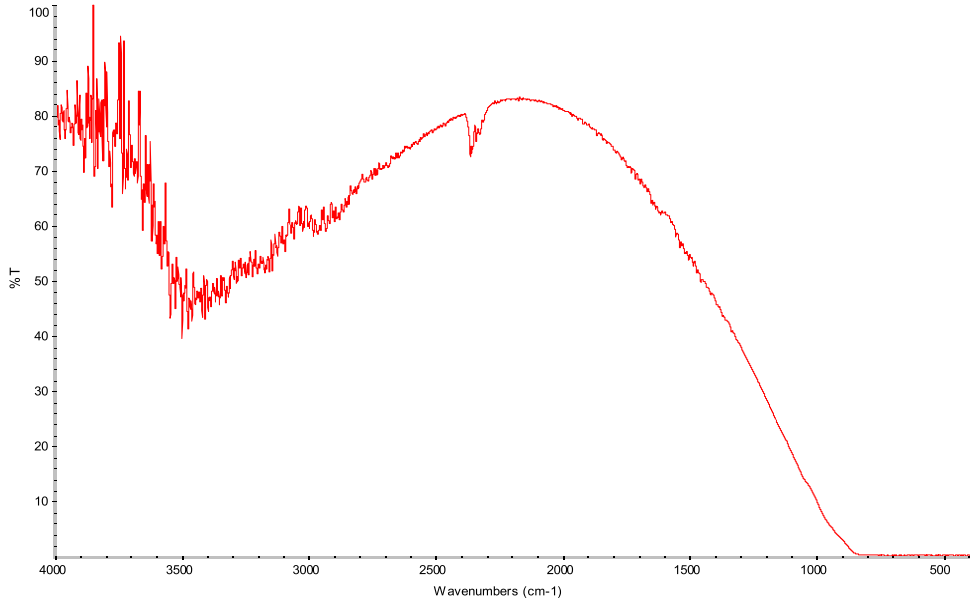


FIGURE 1 | The FTIR curve of K_2CO_3/MgO catalyst.

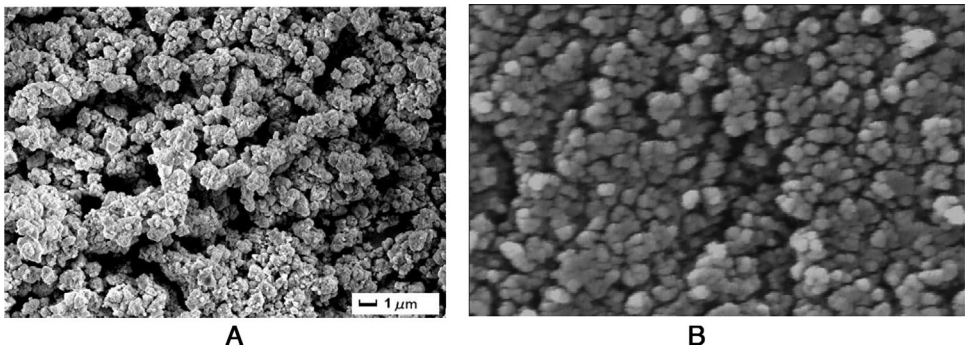


FIGURE 2 | (A) SEM image of K_2CO_3/MgO catalyst. (B) SEM image of MgO alone (the carrier) catalyst.

features: surface morphology, distribution of K_2CO_3, interaction and coverage, and particle size and shape.

Surface morphology; Figure 2A illustrates the surface texture of the MgO particles. MgO presents a porous, rough surface which provides numerous sites for K_2CO_3 deposition. Figure 2A shows K_2CO_3 as distinct particles or layers covering the MgO surface. These particles appeared as bright spots indicating regions where K_2CO_3 is concentrated. Interaction and coverage; Figure 2A also highlights the extent of coverage, showing how uniformly K_2CO_3 is distributed over the MgO. Particle size and shape; Figure 2A provides insights into the size and shape of both the MgO carrier and the K_2CO_3. MgO particles appeared as irregularly shaped agglomerates, while K_2CO_3 particles may appear as smaller, more defined structures.

For comparison, Figure 2B of MgO alone (the carrier) displayed the inherent surface characteristics of the MgO without the K_2CO_3 loading. This image typically shows: porosity and roughness and particle distribution.

Porosity and roughness; Figure 2B shows a porous nature of MgO, with rough surfaces providing high surface area. Particle distribution; Figure 2B shows the spatial distribution and morphology of MgO particles without any modification by K_2CO_3. By comparing Figure 2A,B of SEM images of the K_2CO_3/MgO and MgO as the lone carrier it can been seen that K_2CO_3 modifies the surface, potentially enhancing the functional properties of the MgO carrier.

3.2.2 | CO_2-TPD and XRD Analysis of K_2CO_3/MgO

3.2.2.1 | Influence of K_2CO_3/MgO Ratio of the Starting Materials. The influence of the ratio of K_2CO_3 to MgO of the starting materials on CO_2 adsorption capacities of the prepared samples was examined by performing CO_2 (99.995%) adsorption experiments on a thermogravimetric analyser (TGA) at 375°C (Figure 3). It is clear from Figure 3 that adsorbents with different starting material ratios have different adsorption capacities. At a ratio of 1:2 (DS1), the adsorption amount was about 5.28 wt% increasing to 8.55 wt% when the ratios were increased to 1:3 (DS2). Further increase to 1:4 (DS3), and 1:5 (DS4) did not lead to additional CO_2 adsorption capacity. The ratio of 1:3 was preferred as this minimizes usage of starting materials [33].

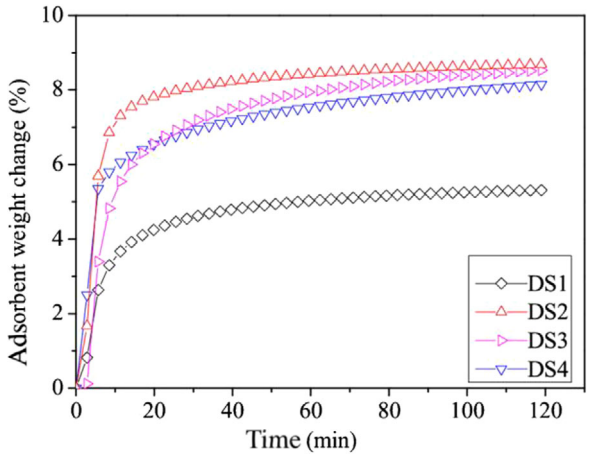


FIGURE 3 | Effect of K:Mg ratio on CO_2 adsorption capacity [31].

3.2.2.2 | XRD Analysis

3.2.2.2.1 | Elemental Analysis. The effect of K:Mg ratio on CO_2 adsorption capacities could be explained from XRD analysis and elemental analysis. XRD patterns show that the adsorption of CO_2 on these samples resulted from the reaction between MgO, K_2CO_3, and CO_2, at the same time, the elemental analysis shows that molar ratios of MgO to K_2CO_3 in DS1, DS2, and DS3 are 1:0.45, 1:0.95, 1:1.06, and 1:0.92, respectively (Figure 4). In DS2, DS3, and DS4 the ratios were close to the stoichiometric ratio of MgO/K_2CO_3 in the reaction, therefore there was no excess of either component which could take up some dead weight of the sample as was the case for DS1 (Figure 4) [33].

3.2.2.2.2 | Structural and Textual Properties. Wide-angle XRD patterns of the prepared samples were collected to analyze phase changes in the samples before and after CO_2 adsorption. All the freshly calcined samples before CO_2 adsorption show two phases: one is MgO and the other is K_2CO_3. However, the relative strength of MgO peaks to K_2CO_3 peaks are different, indicating the ratios of MgO to K_2CO_3 are different in each sample which could be further demonstrated by elemental analysis [34]. The MgO in the samples resulted from the decomposition of $MgCO_3$ in the precipitate at the calcination temperature of 450°C and K_2CO_3 was the stoichiometric excess K_2CO_3 in the precipitate as it did not decompose at 450°C [35]. XRD patterns of the samples after CO_2 adsorption (Figure 4B) illustrate three phases, which are MgO, K_2CO_3, and a new phase which can be indexed as $K_2Mg(CO_3)_2$. The newly formed species, $K_2Mg(CO_3)_2$, also reported by Lee et al. [35, 36] for low temperature CO_2 adsorption in the presence of water vapor using MgO based adsorbents, was the reaction product of MgO, K_2CO_3 with CO_2. There were no $KHCO_3$ or $MgCO_3$ phases found after CO_2 adsorption, in contrast to the results of CO_2 adsorption at 60°C reported by Lee et al. [35, 36], as their respective decomposition temperatures are 100°C to 120°C and 330°C, much lower than the adsorption temperature.

3.2.2.3 | Adsorption at Different Temperatures. Initially, the research suggested a ratio of 1:3 (sample DS2) was sufficient to exhibit good adsorption capacity without excessive use of K_2CO_3 and hence this sample was selected for further analysis. The adsorption of CO_2 at different temperatures was performed on sample DS2. The specific temperatures were chosen because of the appropriate temperature range for CO_2. Figure 5 shows that the weight change of the adsorbent at 300°C is a gradual process increasing slowly with a final CO_2 uptake of 1.2 wt% of the adsorbent. At 350°C and 375°C however, the weight of the adsorbent experienced a rapid increase with final CO_2 uptakes of 8.39 wt% and 8.69 wt% for 350 and 375°C, respectively. Adsorption of CO_2 at 400°C was negligible.

3.2.3 | N2 Adsorption-desorption and Hammett Indicators Analysis of K_2CO_3/MgO

N2 adsorption/desorption isotherms show that the as-prepared adsorbents have a hysteresis loop at p/p0 of 0.8–1.0, indicating large void spaces between crystals (Figure 6). The data calculated by the BET method shows that surface areas of the prepared samples are around 2 m^2/g, which is much lower than most of the adsorbents for physisorption and essentially corresponds to the external surface area of the crystals.

Differential thermogravimetric curves of the four samples were recorded over the temperature range of 25–800°C in nitrogen flow (Figure 7). These curves show that the highest weight loss rate occurred at different temperatures, increasing with the content of K_2CO_3 in the starting material (Figure 7). For DS1, the highest decomposition rate appeared at 331°C, which is the same decomposition temperature as pure $MgCO_3$ [33]. This is expected as $MgCO_3$ is the main phase in this sample since the molar ratio of $MgCO_3$ to K_2CO_3 is 1:0.45. For

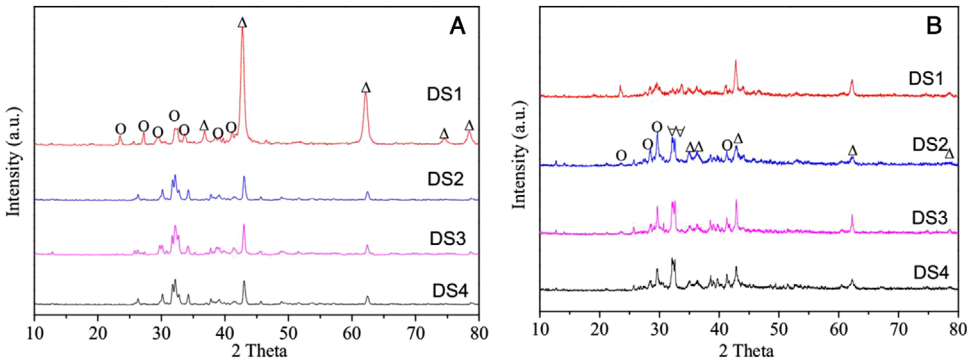


FIGURE 4 | Powder XRD patterns of the samples: (A) before CO_2 adsorption; (B) after CO_2 adsorption: (1) MgO; K_2CO_3 [33].

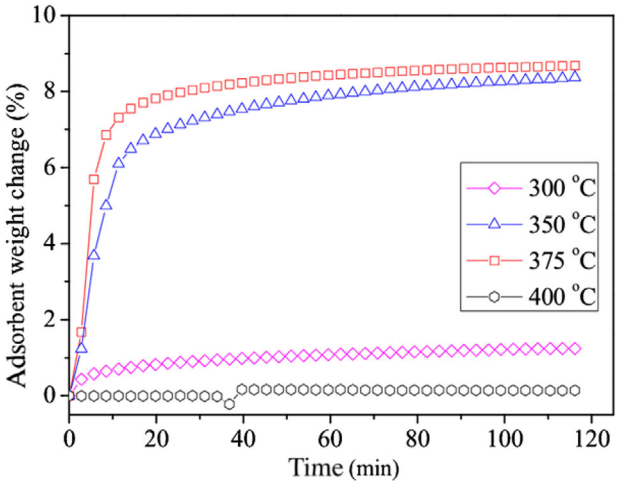


FIGURE 5 | Uptake curves of the adsorption of pure CO_2 at different temperatures on sample DS2 [33].

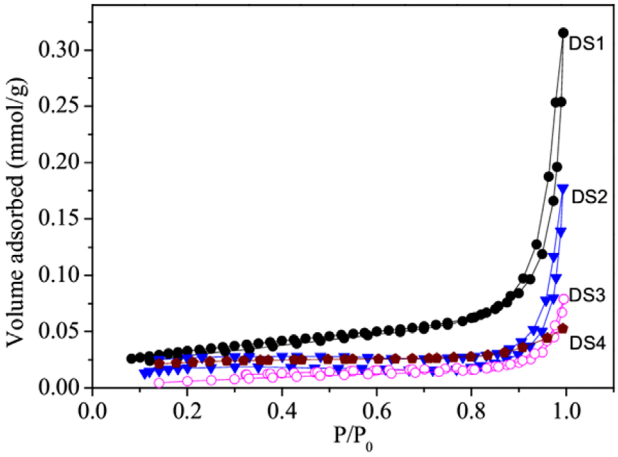


FIGURE 6 | N2 adsorption-desorption isotherms at 77 K for the adsorbent samples [33].

samples with higher potassium content, the corresponding highest rate of decomposition occurred at 388°C for DS2, 423°C for DS3, and 489°C for DS4. The shift of highest weight loss peaks from normal decomposition temperature of $MgCO_3$ to higher temperature is in keeping with the relative increase in K_2CO_3 and its corresponding higher decomposition temperature (K_2CO_3).

3.2.4 | The Strength of Alkalinity of Catalysts

The change of color by the acid-base indicator is in accordance to the surface site strength and $_pK_{BH}$ values of indicators. The strength of the surface basic site is stated in terms of acidity function (H_-) proposed by Paul and Long [36]. The definition of the H_- function is through this equation:

$$H_- = {}_pK_{BH+} \log(B^-)/(BH) \quad (2)$$

where (B^-) and (BH) are the concentration of the indicator and its conjugated base, respectively and $_pK_{BH}$ is the logarithm of the dissociation constant of (BH). The reaction of the indicator BH with the basic site B is:

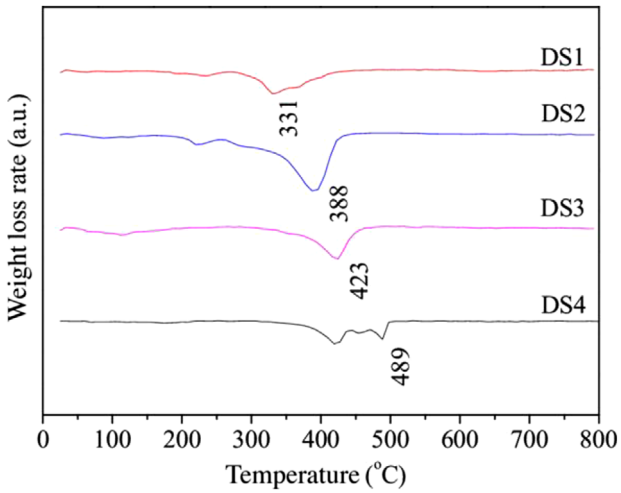


FIGURE 7 | Differential thermogravimetric profiles of adsorbent samples [33].

$$BH + \underline{B} = B^- + \underline{BH}^+ \quad (3)$$

The basic site amounts of various strengths are measured using titration with benzoic acid and basic strength corresponds to the $_pK_{BH}$ value of the indicator used.

The base strength distribution of the K_2CO_3-MgO catalysts were summarized in Table 4. The number of basic sites per unit surface area was determined for certain ranges of base strength (H_-). The base strength distribution was obtained from the color changes of Hammett indicators [37]. The amount of strong basic sites in the range 17.2 (H_-)–26.5(H_-) increases whereas the medium basic sites show the tendency like the surface basicity [38, 39]. It was suggested that moderately basic sites are active for the reaction [40–43]. The results indicate the high concentration of strong basic site can give negative effect on the biodiesel yield by producing by-products (see Table 3).

3.3 | The Effects of Reaction Parameters on Biodiesel Yield

3.3.1 | The Effect of the Loading Ratio of K_2CO_3/MgO on the Reaction

The influence of K_2CO_3/MgO loading ratio for sample DS1, DS2, DS3, DS4, and DS5 of loading ratio; 0.1:2, 0.2:3, 0.4:4, 0.6:5, and 0.8:6 on the transesterification of *P. resiniferum* seed oil using methanol was studied (Figure 8). The reaction progressed efficiently with a yield of 55.4%, 85.8%, 92.6%, and 97.4% at adjustment of loading ratio of K_2CO_3/MgO to 0.6:5 being the maximum yield. Increasing the loading ratio of K_2CO_3/MgO further to 0.8:6, resulted in decrease in the yield to 97.2%.

The findings revealed that the concentration of K_2CO_3 used resulted into a significant impact on the response. With a yield of 15%, a single MgO had weak activity for the reaction, indicating that the reactions' active sites were not exclusively MgO-derived. Active sites on the catalyst were insufficient, thus the reaction

TABLE 3 | Base strength distribution of K_2CO_3-MgO catalysts.

Catalysts	Base strength distribution ($H_$) (%)[a]				
	8.2–10.5	10.5–15.0	15.0–17.2	17.2–18.4	18.4–26.5
1	18.9	22.8	31.2	18.0	9.1
2	14.0	17.2	31.1	27.9	9.8
3	12.1	13.2	26.8	35.6	12.2
4	3.5	5.8	30.8	43.5	16.4

[a]Measured from the color changes of Hammett indicators benzene carboxylic acid.

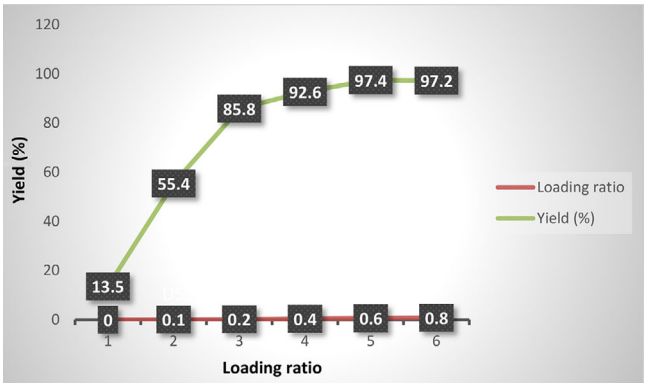


FIGURE 8 | Loading ratio effects on reaction process.

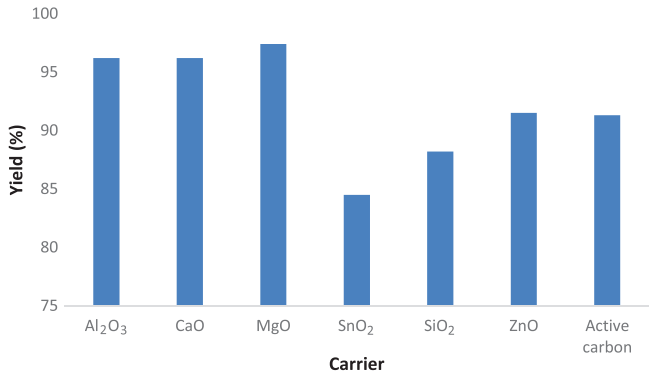


FIGURE 9 | Effect of carrier – catalyst on the reaction.

could not be carried out successfully with a little quantity of K_2CO_3.

3.3.2 | The Effect of the Different Carriers of the Catalyst on the Reaction

Catalytic activity of K_2CO_3 supported by various carriers were explored (Figure 9). The carriers had a positive influence on the reaction with high yields as demonstrated by the result. Basic carriers had greater activity than acidic carriers like SnO_2 and SiO_2, because of the strong contact between K_2CO_3 and the carriers. The solitary CaO also showed a strong activity for the process, with a yield of 83% [31], but the catalytic activity was enhanced significantly when it was supplemented by K_2CO_3. The increased activity of K_2CO_3/Al_2O_3 for the reaction was due to the carrier's high BET surface of 209 m^2/g and the interaction among K_2CO_3 and Al_2O_3, resulting in stronger and more evenly distributed active sites. K_2CO_3/MgO produced the highest yield (97.4%). Although K_2CO_3/CaO has comparable activity, it is susceptible to water and readily converts to hydroxide. As a result, K_2CO_3/MgO was identified to be the most effective catalyst for the reaction process.

TABLE 4 | The effect of molar ratio of methanol-to-oil on the reaction.

Entry	Amount of methanol (g)	Yield (%)
1	0.72	89.6
2	0.93	93.5
3	1.09	97.4
4	1.53	97.2
5	2.30	96.1

3.3.3 | The Effect of the Molar Ratio of the Reactants

The molar ratio of *P. resiniferum* seed oil and methanol was studied (Table 4). The findings revealed an increased in the yield when the amount of methanol was added, with the highest value being attained as the methanol amount was 1.09 g and the molar ratio of methanol to oil was 16:1. It is critical for this type of reaction to increase the quantity of methanol. An excess of methanol could have a dilution effect, causing the reaction to occur at a low temperature.

3.3.4 | The Effect of the Reaction Temperature

Reaction temperatures was varied from 50°C, 55°C, 60°C, and 65°C, while other parameters were kept constant. The parameters kept constant were; time at 2.0 h, molar ratio of methanol to oil at 16:1, and 5% catalyst loading amount.

From Figure 10; the amount of biodiesel produced rose from 87.6% to 92.5% as the temperature was raised from 50°C to 55°C, respectively. The optimum temperature was reached at 60°C with biodiesel yield of 97.4%. Increasing temperature leads to the rise in the rate of reaction during transesterification process and therefore, makes it more efficient. At 65°C, and 70°C the yield sharply decreases to 87.1% and 83.2% respectively. The methanol

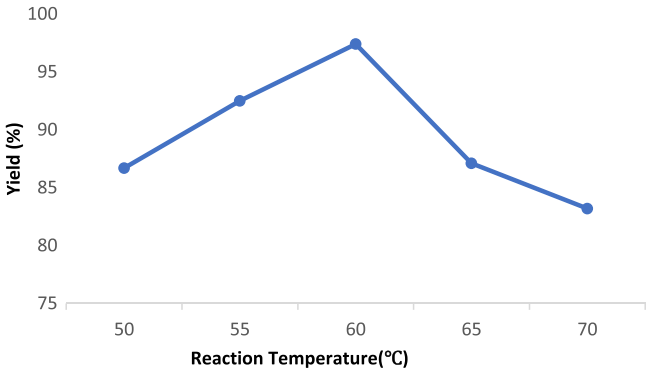


FIGURE 10 | Effect of temperature on the reaction.

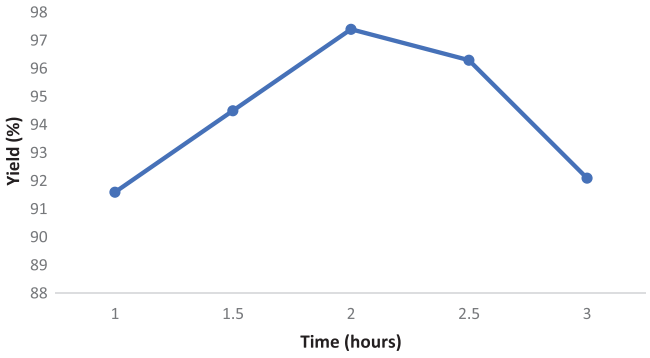


FIGURE 11 | Effect of time on the reaction.

turns into vapor from 65°C and above forming bubbles which inhibit the reaction surface. Gui et al. [40], in their study found similar trends and found out that the reaction temperature should be less than the boiling point of the alcohol to stop leaking through vaporization and depending on the oil used, the optimal temperatures should be between 50°C and 60°C.

3.3.5 | The Effect of the Reaction Time

The function of time on yield was studied (Figure 11). Result shows efficiency of the catalyst for the transesterification process, with a yield of 97.4% within 2.0 h. The reaction was immediate and it steadily increased in intensity until it reached an optimum yield at around 2.0 h, thereafter it decreased. The best reaction time was considered to be 2.0 h and there were three stages of the reaction. Triglycerides were converted into diglycerides, monoglycerides, and glycerol. Catalysts are assumed to have a particular selectivity to diglycerides and monoglycerides.

3.3.6 | The Effect of the Catalyst Amount

The amount of catalyst was considered critical for this reaction. According to Table 5, too low catalyst quantity resulted into insufficient active sites available for the reaction. The reaction is however reversed on application of excess catalyst. An optimum amount of catalyst was 45 mg.

TABLE 5 | The effect of catalyst amount.

Entry	Catalyst amount (mg)	Yield (%)
1	5.0	86.5
2	25	92.6
3	45	97.4
4	65	97.1
5	85	97.2

TABLE 6 | Comparison of different catalysts.

Entry	Catalyst	Catalyst amount (mg)	Yield (%)
1	K_2CO_3/MgO	45	97.4
2	K_2CO_3	55	90.3

TABLE 7 | Reusability of the catalyst.

No. of runs	Yield (%)
1st	97.4
2nd	94.2
3rd	89.5
4th	86.1
5th	83.3

3.3.7 | Catalytic Activities of the Catalyst

A comparison of the catalytic activity of K_2CO_3/MgO and of K_2CO_3 was performed (Table 6). According to the findings, the catalyst outperformed typical heterogenous catalysts in terms of activity (K_2CO_3). The K_2CO_3/MgO catalytic activity was greater compared to that of K_2CO_3. K_2CO_3 and MgO, interactions as well as the high dispersion degree of K_2CO_3 active sites on the surface of MgO, is the primary reason. Furthermore, saponification of the homogeneous catalysts lowered yield. Catalyst should be viewed as one of the top options for a cost-effective, and user-friendly as it is demonstrated clearly. The moisture content of *P. resiniferum* oil was critical in this study. Saponification might occur because of the oil that was used has a water content of 0.64%.

3.3.8 | The Reusability of the Catalyst

Filtering of the catalyst was carried out and calcination at a temperature of 400°C for 4 h after the reactions. The retrieved catalyst was thoroughly probed (Table 7). Even after recycling the catalyst five times, the catalytic activity led to little decrease in the yield from 97.4% to 83.3%. After the reactions, the active sites were filled by the organic species, and the base strength was assessed using the Hammet-index which revealed that the PKa was less than 12, reducing the catalyst's catalytic activity.

TABLE 8 | Comparison of properties of *Pittosporum resiniferum* biodiesel to American and European Union standards.

Fuel properties	Method	*Pittosporum resiniferum* Biodiesel	ASTM D6751	EN 14214
Cetane number	ASTM D6890	52	≥47	≥51
Kinematic viscosity (mm^2/s; 40°C)	ASTM D445	4.3	1.9–6.0	3.5–5.0
Oxidative stability 110°C (h)	EN 14112	2.1	≥3	≥6
Pour point (°C)	GB/T3535	−1	Report[a]	Country specific[a]
Flash point (°C)	ASTM D93	152	≥93	≥120
Sulfur content (%, w/w)	ASTM D4294	0.002	≤0.05	0.020
Ash content (%, w/w)	GB/T508	0.018	≤0.02	≤0.02
Acid value (KOH mg/kg)	ASTM D664-01	0.454	≤0.5	≤0.5
Water (mg/kg)	ASTM D6304	0.04	≤0.05	≤0.05
Density (20°C)	SH/T0248	865	—	860–900
Total glycerine (%, w/w)	SH/T0796	0.14	0.24	≤0.25

[a]Low temperature properties are not strictly specified, but should be agreed upon by the fuel supplier or purchaser.

3.4 | Comparison of *Pittosporum resiniferum* Biodiesel Properties to International Standards

Table 8 compares the attributes of biodiesel to the United States (ASTM D6751) and Europe (EN 14214) standards. In general, the characteristics of biodiesel revealed several similarities with regular diesel. As a result, biodiesel derived from *P. resiniferum* seed oil is regarded as a viable feedstock for producing biodiesel which can be used alternatively in diesel engine.

4 | Conclusions

P. resiniferum oil has not been widely used as a substitute feedstock for producing biodiesel. The study's main aim was to investigate biodiesel production through transesterification of *P. resiniferum* oil using heterogeneous solid base catalyst.

K_2CO_3/MgO, was used as catalyst to produce biodiesel from *P. resiniferum* seed oil. The catalyst was exceptionally efficient for the process resulting into a highest yield of 97.4%. The catalyst and technique of preparation were distinguished by their simplicity in its operation, lack of solvent requirement, low cost, greater yield, rapid reaction time, and its ability to be reused.

Acknowledgments

The authors have nothing to report.

Conflicts of Interest

The authors declare no conflicts of interest.

Data Availability Statement

All the data associated with the research is embedded in the manuscript.

References

1. M. Abid, A. Touzani, and R. Benhima, "Synthesis of Biodiesel From Chicken's Skin Waste by Homogeneous Transesterification," *International Journal of Sustainable Engineering* 12, no. 4 (2019): 272–280, https://doi.org/10.1080/19397038.2018.1521883.

2. S. Ishak and A. Kamari, "A Review of Optimum Conditions of Transesterification Process for Biodiesel Production from Various Feedstocks," *International Journal of Environmental Science and Technology* 16, no. 5 (2019): 2481–2502, https://doi.org/10.1007/s13762-019-02279-6.

3. S. Budžaki, G. Miljić, M. Tišma, S. Sundaram, and V. Hessel, "Is There a Future for Enzymatic Biodiesel Industrial Production in Microreactors?," *Applied Energy* 201, no. 2017 (2017): 124–134, https://doi.org/10.1016/j.apenergy.2017.05.062.

4. N. Mansir, S. H. Teo, U. Rashid, and Y. H. Taufiq-Yap, "Efficient Waste Gallus Domesticus Shell Derived Calcium-Based Catalyst for Biodiesel Production," *Fuel* 211, (2018): 67–75, https://doi.org/10.1016/j.fuel.2017.09.014.

5. N. Mansir, S. H. Teo, U. Rashid, et al., "Modified Waste Egg Shell Derived Bifunctional Catalyst for Biodiesel Production from High FFA Waste Cooking Oil. A Review," *Renewable and Sustainable Energy Reviews* 82, (2018): 3645–3655, https://doi.org/10.1016/j.rser.2017.10.098.

6. R. L. Patel and C. D. Sankhavara, "Biodiesel Production From Karanja Oil and Its Use in Diesel Engine: A Review," *Renewable and Sustainable Energy Reviews* 71, (2017): 464–474, https://doi.org/10.1016/j.rser.2016.12.075.

7. H. M. Mahmudul, F. Y. Hagos, R. Mamat, A. A. Adam, W. F. W. Ishak, and R. Alenezi, "Production, Characterization and Performance of Biodiesel As an Alternative Fuel in Diesel Engines – A Review," *Renewable and Sustainable Energy Reviews* 72, (2017): 497–509, https://doi.org/10.1016/j.rser.2017.01.001.

8. N. D. Priya and M. Thirumarimurugan, "Biodiesel – A Review on Recent Advancements in Production," in *Bioresource Utilization and Bioprocess*, eds. S. K. Ghosh, R. Sen, H. N. Chanakya, A. Pariatamby (Singapore: Springer, 2020), 117–129.

9. V. Makareviciene, E. Sendzikiene, and I. Gaide, "Application of Heterogeneous Catalysis to Biodiesel Synthesis Using Microalgae Oil," *Frontiers of Environmental Science & Engineering* 15, no. 5 (2021). https://doi.org/10.1007/s11783-020-1343-9.

10. M. Kord, S. M. Sadrameli, and B. Ghobadian, "Optimization of Biodiesel Production from Castor Oil Using a Microwave via Response Surface Methodology (RSM)," *Journal of Renewable Energy and Environment* 3, no. 4 (2016): 1–9.

11. C. Sun, F. Qiu, and D. Yang, "Preparation, Characterization of Graphite Oxide Loaded with K_2CO_3 as Heterogeneous Catalyst and Its Transesterification Application," *Arabian Journal for Science and Engineering* 41, no. 1 (2016): 89–96, https://doi.org/10.1007/s13369-015-1575-3.

12. H. Guo, J. Cheng, Y. Mao, et al., "Acid-Base Bifunctional Catalyst with Coordinatively Unsaturated Cobalt-Nitrogen Sites for the Simultaneous Conversion of Microalgal Triglycerides and Free Fatty Acids Into Biodiesel," *Bioresource Technology* 350, (2022): 126862.

13. M. G. Kulkarni, R. Gopinath, L. C. Meher, and A. K. Dalai, "Solid Acid Catalyzed Biodiesel Production by Simultaneous Esterification and Transesterification," *Green Chemistry* 8, no. 12 (2006): 1056–1062.

14. N. Laosiripojana, W. Kiatkittipong, W. Sutthisripok, and S. Assabumrungrat, "Synthesis of Methyl Esters from relevant Palm Products in Near-Critical Methanol with Modified-Zirconia Catalysts," *Bioresource Technology* 101, no. 21 (2010): 8416–8423.

15. S. Sakthivel, S. Halder, and P. D. Gupta, "Optimisation of Process Variables for Production of Biodiesel in Packed Bed Reactor Using Response Surface Methodology," *International Journal of Ambient Energy* 34, no. 2 (2013): 83–91, https://doi.org/10.1080/01430750.2012.740422.

16. X. Liu, H. He, Y. Wang, S. Zhu, and X. Piao, "Transesterification of Soybean Oil to Biodiesel Using CaO as a Solid Base Catalyst," *Fuel* 87, no. 2 (2008): 216–221, https://doi.org/10.1016/j.fuel.2007.04.013.

17. K. Sudsakorn, S. Saiwuttikul, S. Palitsakun, A. Seubsai, and J. Limtrakul, "Biodiesel Production from Jatropha Curcas Oil Using Strontium-Doped CaO/MgO Catalyst," *Journal of Environmental Chemical Engineering* 5, no. 3 (2017): 2845–2852, https://doi.org/10.1016/j.jece.2017.05.033.

18. R. Jothiramalingam and M. K. Wang, "Review of Recent Developments in Solid Acid, Base, and Enzyme Catalysts (Heterogeneous) for Biodiesel Production Via Transesterification," *Industrial & Engineering Chemistry Research* 48, no. 13 (2009): 6162–6172, https://doi.org/10.1021/ie801872t.

19. U. S. P. R. Arachchige, K. A. V. Miyuranga, D. Thilakarathne, R. A. Jayasinghe, and N. A. Weerasekara, "Biodiesel-Alkaline Transesterification Process for Methyl Ester Production," *Nature, Environment and Pollution Technology* 20, no. 5 (2021): 1973–1980, https://doi.org/10.46488/NEPT.2021.V20I05.013.

20. F. Qiu, Y. Li, D. Yang, X. Li, and P. Sun, "Heterogeneous Solid Base Nanocatalyst: Preparation, Characterization and Application in Biodiesel Production," *Bioresource Technology* 102, no. 5 (2011): 4150–4156, https://doi.org/10.1016/j.biortech.2010.12.071.

21. M. Takase, M. Zhang, W. Feng, et al., "Application of Zirconia Modified with KOH as Heterogeneous Solid Base Catalyst to New Non-Edible Oil for Biodiesel," *Energy Conversion and Management* 80, (2014): 117–125.

22. P. M. M. Millena, "Parametric Study on Solvent Extraction of Oil from Petroleum Nut (*Pittosporum resiniferum* Hemsl.) Using Hexane as Solvent" (Undergraduate Theses, University Knowledge Digital Repository, 2016), https://www.ukdr.uplb.edu.ph/etd-undergrad/5422.

23. P. F. Del Rosario, M. M. E. Ignacio, and C. R. Lumanog, "Evaluation of the Physicochemical Properties of Petroleum Nut (*Pittosporum resiniferum*) oil" (Bachelor's Thesis, De La Salle University, 2016), https://animorepository.dlsu.edu.ph/etd_bachelors/7269.

24. J. Pirker, A. Mosnier, F. Kraxner, P. Havlík, and M. Obersteiner, "What are the Limits to Oil Palm Expansion?," *Global Environmental Change* 40, (2016): 73–81, https://doi.org/10.1016/j.gloenvcha.2016.06.007.

25. A. R. Zainal Kifli, S. H. Kamarullah, S. N. Mohd Khazaai, and G. P. Maniam, "Synthesis of Alumina-CaO-KI Catalyst for the Production of Biodiesel from Rubber Seed Oil," *Malaysian Journal of Analytical Sciences* 22, no. 2 (2018): 279–285, https://doi.org/10.17576/mjas-2018-2202-13.

26. W. Xie and H. Li, "Alumina-Supported Potassium Iodide as a Heterogeneous Catalyst for Biodiesel Production from Soybean Oil," *Journal of Molecular Catalysis A: Chemical* 255, no. 1-2 (2006): 1–9.

27. F. Li, L. Yang, T. Zhao, et al., "Optimization of Enzymatic Pretreatment for n-Hexane Extraction of oil from Silybum Marianum Seeds Using Response Surface Methodology," *Food and Bioproducts Processing* 90, no. 2 (2012): 87–94.

28. J. P. Da Costa Evangelista, A. D. Gondim, L. Di Souza, and A. S. Araujo, "Alumina-Supported Potassium Compounds as Heterogeneous Catalysts for Biodiesel Production: A Review," *Renewable and Sustainable Energy Reviews* 59, (2016): 887–894, https://doi.org/10.1016/j.rser.2016.01.061.

29. Y. Pourbakhshi, M. Farhadian, A. Bahrami, L. Tajik, F. Ghorbani Shanha, and M. J. Assari, "Application of Artificial Neural Network and Response Surface Methodology in Optimization of Cold Fiber Headspace Solid-Phase Microextraction (CF-HS-SPME) for Analysis of 2, 5-Hexandion in Urine Samples," *Jundishapur Journal of Health Sciences* 12, no. 3 (2020). https://doi.org/10.5812/jjhs.100925.

30. L. F. Chuah, J. J. Klemeš, A. Bokhari, and S. Asif, "A Review of Biodiesel Production from Renewable Resources: Chemical Reactions," *Chemical Engineering Transactions* 88 (May 2021): 943–948, https://doi.org/10.3303/CET2188157.

31. R. D. Lanjekar and D. Deshmukh, "A Review of the Effect of the Composition of Biodiesel on NOx Emission, Oxidative Stability and Cold Flow Properties," *Renewable and Sustainable Energy Reviews* 54 (2016): 1401–1411, https://doi.org/10.1016/j.rser.2015.10.034.

32. J. Huang, Y. Zou, M. Yaseen, et al., "Fabrication of Hollow Cage-Like CaO Catalyst for the Enhanced Biodiesel Production Via Transesterification of Soybean Oil and Methanol," *Fuel* 290 (2021): 119799.

33. N. S. El-Gendy, A. Hamdy, A. Hamdy, and S. S. A. Amr, "An Investigation of Biodiesel Production from Wastes of Seafood Restaurants," *International Journal of Biomaterials* (2014). https://doi.org/10.1155/2014/609624.

34. G. Xiao, R. Singh, A. Chaffee, and P. Webley, "Advanced Adsorbents Based on MgO and K_2CO_3 for Capture of CO_2 at Elevated Temperatures," *International Journal of Greenhouse Gas Control [Internet]* 5, no. 4 (2011): 634–639, http://doi.org/10.1016/j.ijggc.2011.04.002.

35. K. H. Stern, *High Temperature Properties and Thermal Decomposition of Inorganic Salts with Oxyanions*, 1st ed. (Boca Raton, FL: CRC Press, 2000).

36. K. B. Lee, M. G. Beaver, H. S. Caram, and S. Sircar, "Reversible Chemisorbents for Carbon Dioxide and Their Potential Applications," *Industrial & Engineering Chemistry Research* 47, no. 21 (2008): 8048–8062.

37. S. C. Lee, H. J. Chae, S. J. Lee, et al., "Development of Regenerable MgO-Based Sorbent Promoted With K_2CO_3 for CO_2 Capture at Low Temperatures," *Environmental Science & Technology* 42, no. 8 (2008): 2736–2741.

38. F. A. Long and M. A. Paul, "Application of the H0 Acidity Function to Kinetics and Mechanisms of Acid Catalysis," *Chemical Reviews* 57, no. 5 (1957): 935–1010.

39. B. M. Bhanage, S. Fujita, Y. Ikushima, and M. Arai, "Synthesis of Dimethyl Carbonate and Glycols from Carbon Dioxide, Epoxides, and Methanol using Heterogeneous Basic Metal Oxide Catalysts with High Activity and Selectivity," *Applied Catalysis A* 219, (2001): 259.

40. Y. Watanabe and T. Tatsumi, "Hydrotalcite-Type Materials as Catalysts for the Synthesis of Dimethyl Carbonate from Ethylene Carbonate and Methanol," *Microporous and Mesoporous Materials* 22, (1998): 259.

41. M. M. Gui, K. T. Ã. Lee, and S. Bhatia, "Feasibility of Edible Oil vs. Non-Edible Oil vs. Waste Edible Oil as Biodiesel Feedstock," *Energy* 33, no. 11 (2008): 1646–1653, https://doi.org/10.1016/j.energy.2008.06.002.

42. L. Zhu, X. Q. Liu, H. L. Jiang, and L. B. Sun, "Metal-Organic Frameworks for Heterogeneous Basic Catalysis," *Chemical Reviews* 117, no. 12 (2017): 8129–8176, https://doi.org/10.1021/acs.chemrev.7b00091.

43. H. Abimanyu, C. S. Kim, B. S. Ahn, and K. S. Yoo, "Synthesis of Dimethyl Carbonate by Transesterification With Various MgO-CeO2 Mixed Oxide Catalysts," *Catalysis Letters* 118, no. 1–2 (2007): 30–35, https://doi.org/10.1007/s10562-007-9091-z.